A Theoretical Study of the Ion−Molecule Chemistry of $K^+ \cdot X$ Complexes (X = O, O_2, N_2, CO_2, H_2O): Implications for the Upper Atmosphere†

John M. C. Plane,*,‡ Richard J. Plowright,§ and Timothy G. Wright*,§

School of Environmental Sciences, University of East Anglia, Norwich NR4 7TJ, U.K., and School of Chemistry, University of Nottingham, University Park, Nottingham NG7 2RD, U.K.

Received: August 8, 2005; In Final Form: October 4, 2005

High-level ab initio calculations were carried out on a series of $K^+ \cdot X$ cluster ions (X = O, O_2, N_2, CO_2, H_2O) and $X \cdot K^+ \cdot Y$ ions. Rice−Ramsberger−Kassel−Markus theory was then used to estimate the rate coefficients for a series of recombination and ligand-switching reactions that govern the ion−molecule chemistry of K^+ in the upper mesosphere and lower thermosphere. These rate coefficients were then included in an atmospheric model of potassium chemistry. The important result is that K^+ forms weakly bound clusters with N_2, O_2, and O (the major atmospheric species), with binding energies between 10 and 22 kJ mol^{-1}. Even under atmospheric conditions (200 K and 10^{-3} Torr), these cluster dissociate in less than 1 s. This prevents the formation by ligand-switching of the more stable CO_2 and H_2O clusters, which could then undergo dissociative recombination with electrons to produce K. The result is that K^+ ions have a much longer lifetime against neutralization in the upper atmosphere than other metallic ions such as Na^+ and Fe^+.

1. Introduction

The major source of potassium in the upper mesosphere and lower thermosphere (MLT) is the ablation of the 20−50 tons of interplanetary dust that enters the atmosphere each day.[1] This gives rise to a layer of K atoms between 80 and 105 km that is global in extent. At midlatitudes, the K layer has a full width at half-maximum of about 9 km and a peak concentration of 50−60 cm^{-3} at a height of about 88 km.[2] The layer has been observed by solar-pumped resonance fluorescence during twilight[3−5] and by resonant lidar (laser radar) operating on the D$_1$ line at 769.9 nm [K($4^2P_{1/2}$−$4^2S_{1/2}$)].[2,6−11] Lidar measurements have also confirmed the presence of K atoms in fresh meteor trails.[12−15] K^+ ions have been observed by rocket-borne mass spectrometry.[16−22] Although only about 15 rocket flight measurements have been reported, there appears to be a permanent layer of K^+ ions above 90 km, with a concentrations up to ∼100 cm^{-3}. This background ion concentration can be considerably enhanced, by more than 1 order of magnitude, in a sporadic E layer.[22]

In this paper we describe a theoretical study of the ion−molecule chemistry of potassium, to understand how K^+ and K are coupled in the MLT. The application of theory is required because the only experimental studies appear to have been of the reactions of K^+ with O_3[23] and with O_2 and H_2O.[24] No kinetic studies of reactions involving K^+ cluster ions have been reported. The reasons for exploring this chemistry in detail are to model the diurnal variation of the topside of the global K layer[2] and to understand the very interesting phenomenon of sporadic potassium layers (K_s). K_s are thin layers of K atoms (∼1−3 km wide) that occur at altitudes between 90 and 105 km and can appear and disappear within a few minutes.[10] The first sporadic layers to be discovered were Na_s, and these have now been quite extensively studied.[25−28] The most promising explanation for Na_s formation is the neutralization of Na^+ ions concentrated in a sporadic E layer (E_s). The observational evidence for this is the high correlation in time and space between Na_s and E_s.[25,26,28,29] An atmospheric model of sodium ion−molecule chemistry,[30] developed from laboratory kinetic measurements[31] and quantum theory calculations,[32] has been used to reproduce several case studies of Na_s formation.[28,29]

K^+ ions form directly in the MLT via hyperthermal collisions (impact energy > 4 eV) between ablating K atoms and air molecules.[33] However, they also form continuously from K atoms in the background layer, via photoionization,[34] and charge transfer with ambient ions:[2]

$$K + h\nu \rightarrow K^+ + e^- \quad (1)$$

$$K + NO^+ \rightarrow K^+ + NO \quad (2)$$

$$K + O_2^+ \rightarrow K^+ + O_2 \quad (3)$$

The rate of charge transfer dominates and exhibits a large diurnal variation because the daytime plasma density increases by roughly 1 order of magnitude.[1] Hunten[35] suggested that another source of K^+ might be Penning ionization: $K + O_2(^1\Delta_g) \rightarrow K^+ + O_2 + e^-$. However, this process still requires 3.35 eV of energy and so will be virtually nonexistent at the low temperatures in the MLT.

Neutralization of K^+ can occur through radiative recombination with electrons ($K^+ + e^- \rightarrow K + h\nu$), but this is very inefficient.[36] Instead, K^+ must first complex with a ligand X, where X = N_2, O_2, O, CO_2, or H_2O (in order of decreasing atmospheric concentration), and then perhaps undergo ligand-switching with another atmospheric component Y to form a more stable complex, before undergoing dissociative electron

† Part of the special issue "Jürgen Troe Festschrift".
* To whom correspondence should be addressed.
‡ University of East Anglia.
§ University of Nottingham.

10.1021/jp054416g CCC: $33.50
Published on Web 11/09/2005

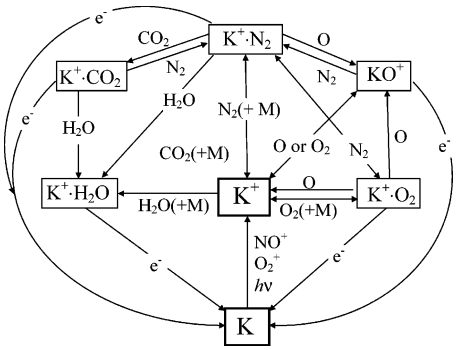

Figure 1. Schematic diagram of the ion−molecule chemistry of potassium in the upper atmosphere. (Some minor pathways are omitted for clarity.)

recombination:

$$K^+ + X\,(+M) \rightarrow K^+\cdot X$$

$$K^+\cdot X + Y \rightarrow K^+\cdot Y + X$$

$$K^+\cdot Y + e^- \rightarrow K + Y$$

Here M is a third body (most likely N_2 or O_2). Figure 1 illustrates schematically most of the chemical pathways that couple K^+ and K in the MLT.

In this paper we report ab initio quantum calculations on the $K^+\cdot X$ complexes at a high level of theory. Optimized geometries and hence rotational constants for the complexes were obtained, and these, together with the harmonic vibrational frequencies and total energies, were used as input for Rice−Ramsberger−Kassel−Markus (RRKM) calculations to estimate rate coefficients for the recombination reactions between K^+ and X, the unimolecular dissociation reactions of the $K^+\cdot X$ complexes, and a series of ligand-switching reactions. These were then incorporated into an atmospheric model to determine the vertical profiles of potassium-containing ions in the MLT and the lifetime of K^+ against neutralization.

2. Ab Initio Calculations on the K^+ Cluster Ions

2.1. $K^+\cdot X$ Species. Calculations on the $K^+\cdot X$ species (geometry optimizations, rotational constants, and vibrational frequency calculations) have been reported in detail previously by us, and so we only overview them here. $K^+\cdot N_2$ and $K^+\cdot CO_2$ were both found to be linear,[37] while $K^+\cdot H_2O$ was most stable with the K^+ positioned along the C_2 axis, interacting with the oxygen atom;[37] these three species are closed-shell singlets. The $K^+\cdot O_2$ complex is also linear with a $^3\Sigma^-$ ground state.[38] Neutral KO_2 is a largely ionic stable molecule with a Coulombic interaction between K^+ and O_2^-. Ionization amounts essentially to loss of an electron from O_2^- and the formation of the weakly bound $K^+\cdot O_2$ complex. In a similar way, the $K^+\cdot O$ complex is formed upon ionization of the KO molecule and is also a $^3\Sigma^-$ state.[39]

The geometries and vibrational frequencies at the highest levels of theory reported in each of the cited papers were used in this work (these had been obtained using a LANL2 ECP coupled with a valence basis set for K^+). At those optimized geometries, single-point calculations were carried out at the RCCSD(T) level of theory. The basis sets employed were the aug-cc-pV5Z basis sets for all first row atoms, but with the *h* functions omitted. For K^+, we employed our own basis set which uses the ECP10MWB effective core potential to describe the 1s−2p electrons and a valence basis set that is similar in form to the aug-cc-pV5Z basis set. The contraction coefficients were obtained from Hartree−Fock calculations on the cation, and the primitive basis functions were constructed in an even-tempered fashion. The full details and performance of this potassium basis set have been described in earlier publications.[37−39] Table 1 lists the relevant parameters required for the application of the reaction rate theories described in sections 3 and 4. The estimated error in the ligand binding energies at this level of theory is typically 1 kcal mol^{-1} (±4 kJ mol^{-1}), based on previous experience; however, the error may be a little larger in cases where there are low intermolecular vibrational frequencies. Note that the weak binding energies of the $K^+\cdot O$ and $K^+\cdot O_2$ ions are consistent with the observed lack of a fast bimolecular reaction between K^+ and O_3.[23]

2.2. Intermediate Cluster Ions. The binding energies, vibrational frequencies, and rotational constants of the intermediate cluster ions formed during ligand-switching, $X\cdot K^+\cdot Y$ were calculated. These species are bound by charge-dipole and charge/charge-induced-dipole interactions. The required quantities were obtained by carrying out low-level initial optimizations, followed by MP2 and B3LYP geometry optimizations. For these, the standard aug-cc-pVTZ basis set was used for all atoms except for K, where our LANL2-(8s8p4d2f) basis set was employed—this has the LANL2 effective core potential, but the valence basis set is replaced with one we developed previously[39] to be similar in form to an aug-cc-pVTZ basis set. For simplicity, we simply refer to "aug-cc-pVTZ" below.

Two of the exchange reactions, $K^+\cdot CO_2 + N_2 \rightarrow K^+\cdot N_2 + CO_2$ and $K^+\cdot O + N_2 \rightarrow K^+\cdot N_2 + O$, are particularly important in controlling the rate at which K^+ is neutralized in the atmosphere. Geometry optimizations on $N_2\cdot K^+\cdot CO_2$ and $O\cdot K^+\cdot N_2$ were therefore also performed at the QCISD level, that is, at the same level of theory as for the monoligated cluster ions. For the $O\cdot K^+\cdot N_2$ complex, we considered both end-on and sideways binding of the N_2. However, at the three levels of theory employed the linear structure was always the minimum. At the MP2 level of theory, the side-on approach of N_2 was a $^3A_2$ saddle point, lying ca. 1400 cm^{-1} above the $^3\Sigma^-$ linear minimum, where the open-shell nature arises from the unpaired electrons on the O atom. The QCISD-optimized geometry was

TABLE 1: Total Energies, Spectroscopic Parameters, and Binding Energies for the $K^+\cdot X$ Complexes

species	energy[a]	rotatonl consts[b]	vibrationl freq[c]	binding energy[d]
$K^+\cdot O_2(^3\Sigma^-)$	−178.373 649	2.31	42 (π), 102 (σ), 1646 (σ)	12.1
$K^+\cdot O(^3\Sigma^-)$	−103.188 074	5.07	129 (σ)	17.6
$K^+\cdot N_2(^1\Sigma^+)$	−137.602 825	2.43	135 (σ), 177 (π), 2350 (σ)	18.3
$K^+\cdot CO_2(^1\Sigma^+)$	−216.596 179	1.46	76 (π), 144 (σ), 664 (π), 1349 (σ), 2349 (σ)	34.1
$K^+\cdot H_2O(^1A_1)$	−104.578 742	436.3, 5.75, 5.65	218, 358, 368, 1663, 3820, 3914	64.2

[a] Energies in hartrees, at the (R)CCSD(T)/ECP10MWB[10s9p6d4f3g] level of theory. $E(K^+)$ = −28.182 116 E_h, $E(O_2)$ = −188.400 496 E_h, $E(O)$ = −74.999 394 E_h, $E(N_2)$ = −109.413 094 E_h, $E(CO_2)$ = −188.400 496 E_h, and $E(H_2O)$ = −76.369 127 E_h. [b] In GHz. [c] In cm^{-1}. [d] At 0 K, in kJ mol^{-1}. Zero-point energies of ligands, in kJ mol^{-1}: 9.48 (O_2); 14.1 (N_2); 30.4 (CO_2); 54.0 (H_2O).

TABLE 2: Calculated Geometry and Vibrational Frequencies for O·K^+·N_2 ($X^3\Sigma^-$)[a]

method[a]	R_{NN}/Å	R_{KN}/Å	R_{KO}/Å	energy/E_h	vibrationl freq/cm^{-1}
B3LYP	1.090	2.962	2.992	−212.657 461	4.3 (π), 93.9 (σ), 107.2 (π), 132.6 (σ), 2455.4 (σ)
MP2	1.114	2.924	2.970	−212.288 871	2.7 (π), 98.8 (σ), 105.7 (π), 140.4 (σ), 2191.9 (σ)
QCISD	1.097	2.948	2.981	−212.321 915	
RCCSD(T)	[b]	[b]	[b]	−212.608 453	

[a] For details and basis sets employed, see text. [b] Single-point calculation at the QCISD-optimized geometry.

TABLE 3: Calculated Geometry and Vibrational Frequencies for N_2·K^+·O^2CO^1 ($X^1\Sigma^+$)[a]

method[a]	R_{O1C}/Å	R_{OC2}/Å	R_{OK}/Å	R_{KN}/Å	R_{NN}/Å	energy/E_h	vibrationl freq/cm^{-1}
B3LYP	1.148	1.172	2.688	2.973	1.090	−326.233 341	9.5 (π), 66.0 (π), 87.2 (σ), 106.5 (π), 146.8 (σ), 666.0 (π), 1372.8 (σ), 2417.7 (σ), 2455.0 (σ)
MP2	1.158	1.181	2.664	2.930	1.114	−325.658 486	2.9 (π), 64.2 (π), 91.9 (σ), 104.1 (π), 154.6 (σ), 652.2 (π), 1333.1 (σ), 2192.0 (σ), 2416.8 (σ)
QCISD	1.149	1.174	2.676	2.951	1.097	−325.667 462	
RCCSD(T)	[b]	[b]	[b]	[b]	[b]	−326.016 175	

[a] For details and basis sets employed, see text. [b] Single-point calculation at the QCISD-optimized geometry.

TABLE 4: Calculated Energies, Rotational Constants, and Vibrational Frequencies for the Y·K^+·X Intermediates[a,b]

X, Y	MP2 energy/E_h	rotationl consts (GHz)	vibrationl freq/cm^{-1}
H_2O, CO_2	−292.641 314	436.62, 0.77, 0.74	17.8 (b_2), 18.4 (b_1), 62.0 (b_2), 62.3 (b_1), 111.0 (a_1), 212.3 (a_1), 342.0 (b_1), 358.7 (b_2), 666.6 (b_1), 666.6 (b_2), 1373.2 (a_1), 1664.2 (a_1), 2417.1 (a_1), 3776.5 (a_1), 3855.2 (b_2)
H_2O, O_2	−254.431 995	436.38, 1.04, 1.04	18.5 (b_2), 18.9 (b_1), 42.7 (b_1), 42.8 (b_2), 82.2 (a_1), 213.8 (a_1), 346.4 (b_1), 365.7 (b_2), 1637.5 (a_1), 1664.8 (a_1), 3775.3 (a_1), 3853.4 (b_2)
H_2O, N_2	−213.679 171	436.56, 1.11, 1.11	17.9 (b_2), 18.6 (b_1), 96.3 (a_1), 103.8 (b_2), 104.0 (b_1), 212.8 (a_1), 344.9 (b_1), 363.7 (b_2), 1664.6 (a_1), 2454.7 (a_1), 3775.8 (a_1), 3854.1 (b_2)
O_2, CO_2	−366.411 127	0.48, 0.48	9.4 (π), 9.4 (π), 41.4 (π), 41.4 (π), 66.3 (π), 66.3 (π), 76.1 (σ), 143.6 (σ), 665.8 (π), 665.8 (π), 1373.0 (σ), 1638.3 (σ), 2418.0 (σ)
O_2, N_2	−287.448 342	0.68, 0.68	7.1 (π), 7.1 (π), 44.6 (π), 44.6 (π), 77.5 (σ), 107.8 (π), 107.8 (π), 124.4 (σ), 1637.8 (σ), 2455.5 (σ)
O, CO_2	−291.251 599	0.74, 0.74	6.1 (π), 6.1 (π), 65.7 (π), 65.7 (π), 97.4 (σ), 146.7 (σ), 665.8 (π), 665.8 (π), 1372.9 (σ), 2417.9 (σ)
O, H_2O	−179.272 389	436.49, 1.84, 1.83	15.4 (b_2), 15.8 (b_1), 105.7 (a_1), 212.9 (a_1), 350.0 (b_1), 366.3 (b_2), 1665.5 (a_1), 3774.3 (a_1), 3852.1 (b_2)
O, O_2	−253.041 379	0.98, 0.98	12.4 (π), 13.5 (π), 24.7 (σ), 43.4 (π), 43.4 (π), 99.5 (σ), 1638.4 (σ)

[a] Rotational constants are those calculated at the MP2/aug-cc-pVTZ level of theory; vibrational frequencies are those calculated at the B3LYP/aug-cc-pVTZ level of theory. The symmetries of the vibrational are given in terms of either C_{2v} or $C_{\infty v}$ labels. For the linear complexes there are only two rotational constants. [b] The corresponding MP2 energies (E_h) for the 1:1 complexes and the ligands were calculated at the same geometries as used in Table 1 and were as follows: K^+·H_2O (−104.307 092), K^+·CO_2 (−216.285 660), K^+·N_2 (−137.320 333), K^+·O_2 (−178.075 061), K^+·O (−102.916 018), H_2O (−76.328 958), CO_2 (−188.321 234), N_2 (−109.364 164), O_2 (−150.120 596), O (−74.959 294).

used to obtain the rotational constants for the RRKM calculations. Vibrational frequencies were calculated at the MP2 and B3LYP level of theory; the better agreement of the B3LYP geometries with the QCISD ones led us to use the B3LYP vibrational frequencies in the RRKM calculations. A further RCCSD(T)/aug-cc-pV5Z single point calculation was performed at the QCISD-optimized geometry to obtain more accurate energies. The relevant parameters are given in Table 2. The binding energy of O to K^+·N_2 is 16.0 kJ mol^{-1}.

For the N_2·K^+·CO_2 intermediate either, or both, ligands could approach end-on or side-on. However, as we have found previously with CO_2 ligands binding to cations, the side-on approach is unstable as the $\delta+$ carbon atom is repelled by the cation. Thus, the CO_2 was constrained to approach end-on, and optimizations were carried out for the N_2 being in the two orientations. As with the O·K^+·N_2 intermediate, the side-on approach was found to be a saddle point at the three levels of theory attempted, lying 1350 cm^{-1} above the linear $^1\Sigma^+$ minimum. The linear QCISD-optimized geometry was used to obtain the rotational constants for the statistical mechanics calculations. Vibrational frequencies were calculated at the MP2 and B3LYP level of theory; again, the better agreement of the B3LYP geometries with the QCISD ones led us to use the B3LYP vibrational frequencies in the RRKM calculations. A further RCCSD(T)/aug-cc-pV5Z single point calculation was performed at the QCISD-optimized geometry to obtain more accurate energetics. The relevant parameters are given in Table 3. The binding energy of CO_2 to K^+·N_2 is 32.2 kJ mol^{-1}.

Table 4 lists the parameters for all the other intermediate cluster ions, where MP2 energies were used to calculate the binding energies and B3LYP vibrational frequencies and MP2 geometries were used for the RRKM calculations. The lowest energy isomer only was used in each case, and as can be seen, these were linear except for the cases involving water, where the lowest energy geometries were C_{2v}.

3. RRKM Calculations on the K^+ + X Recombination Reactions

The following recombination reactions of K^+ could be important in the MLT:

$$K^+ + N_2\,(+M) \rightarrow K^+\cdot N_2 \quad (4)$$

$$K^+ + O_2\,(+M) \rightarrow K^+\cdot O_2 \quad (5)$$

$$K^+ + O\,(+M) \rightarrow K^+\cdot O \quad (6)$$

$$K^+ + CO_2\,(+M) \rightarrow K^+\cdot CO_2 \quad (7)$$

$$K^+ + H_2O\,(+M) \rightarrow K^+\cdot H_2O \quad (8)$$

To estimate the rate coefficients k_{4-8} over the temperature range (120−240 K) and pressure range (<1 mTorr) characteristic of the MLT, we now apply RRKM theory using a master equation (ME) formalism based on the inverse Laplace transform method.[40] We have recently described the application of this

TABLE 5: Fitted Parameters for the RRKM Calculations on Reactions 5−9

reacn	k_{rec}[a]/cm^3 molecule^{-1} s^{-1}	$\langle\Delta E\rangle_{down}$[b]/cm^{-1}	$k_{rec,0}$[c]/cm^6 molecule^{-2} s^{-1}	$k_{diss,0}$[d]/cm^3 molecule^{-1} s^{-1}
$K^+ + N_2 + He$	7.65×10^{-10}	200	5.7×10^{-31} $(T/200\ K)^{-2.39}$	7.1×10^{-9} exp(−1680/T)
$K^+ + O_2 + He$	7.07×10^{-10}	200	3.1×10^{-31} $(T/200\ K)^{-2.12}$	3.6×10^{-10} exp(−821/T)
$K^+ + O + He$	6.23×10^{-10}	200	2.2×10^{-32} $(T/200\ K)^{-1.28}$	6.6×10^{-11} exp(−1810/T)
$K^+ + CO_2 + He$	8.79×10^{-10}	100	3.3×10^{-30} $(T/200\ K)^{-2.43}$	3.5×10^{-8} exp(−3470/T)
$K^+ + H_2O + He$	1.81×10^{-9} exp(74/T)	100	7.5×10^{-30} $(T/200\ K)^{-2.22}$	2.4×10^{-7} exp(−7380/T)

[a] High-pressure limiting association rate coefficient. [b] For He as third body, at 300 K. [c] Low-pressure limiting association rate coefficient. [d] Low-pressure limiting dissociation rate coefficient.

formalism to recombination reactions of metallic species,[41] so only a brief description is given here. The reactions are assumed to proceed via the formation of an excited adduct ($K^+ \cdot X^*$), which could either dissociate or be stabilized by collision with the third body, M. Here we take M as He, to compare with experiment. The internal energy of the adduct was divided into a contiguous set of grains (width 15 cm^{-1}), each containing a bundle of rovibrational states. Each grain was then assigned a set of microcanonical rate coefficients for dissociation, which were determined using inverse Laplace transformation to link them directly to $k_{rec,\infty}$, the high-pressure limit recombination coefficient.[40] In the case of these ion−molecule reactions, $k_{rec,\infty}$ was calculated using Langevin theory. For reaction 8, the ion−dipole interaction between K^+ and H_2O was included using the statistical adiabatic channel treatment of Troe.[42] $k_{rec,\infty}$ was then expressed in the Arrhenius form, $A_\infty \exp(-E_\infty/RT)$; the results are listed in Table 5.

The density of states of the adduct was calculated with the Beyer−Swinehart algorithm[43] for the vibrational modes (without making a correction for anharmonicity) and a classical densities of states treatment for the rotational modes. The molecular parameters listed in Table 2 were used. In the case of reactions 4, 5, and 7, the lowest frequency degenerate bending mode (π symmetry) of the adduct was treated as a 2-dimensional free rotor. For reaction 8, the out-of-plane and in-plane rocking modes of the H_2O (218 and 368 cm^{-1}) were also treated as a 2-dimensional free rotor. We have shown elsewhere, using trajectory calculations, that this is a good approximation because of the very long range intermolecular forces that govern these reactions.[31]

The ME describes the evolution with time of the adduct grain populations. The probability of collisional transfer between grains was estimated using the exponential down model, where the average energy for downward transitions, $\langle\Delta E\rangle_{down}$, was an adjustable parameter between 100 and 200 cm^{-1} for He at 300 K.[43] The collision frequency between the adduct and He was calculated from Langevin theory, yielding $\sim 5.4 \times 10^{-10}$ cm^3 molecule^{-1} s^{-1} for the five reactions. To use the ME to simulate irreversible stabilization of the adduct, an absorbing boundary was set 10 kJ mol^{-1} below the energy of the reactants, so that collisional energization from the boundary to the threshold was highly improbable. The ME was then expressed in matrix form[40] and solved to yield the recombination rate constant at a specified pressure and temperature. Note that all five reactions were found to be essentially at their low-pressure limits at a pressure of 10^{-3} Torr.

Reaction 4 is likely to be the most important of these association reactions in the MLT, because N_2 is the most abundant potential ligand. Although reaction 4 has not been studied experimentally, we have measured the rate coefficient for the analogous reaction of Na^+, obtaining $k(Na^+ + N_2 + He, 93-255\ K) = (1.20 \pm 0.13) \times 10^{-30}$ $(T/200\ K)^{-(2.20\pm0.09)}$ cm^6 molecule^{-2} s^{-1}.[31] If we apply the RRKM formalism described above to this reaction, using the molecular parameters for $Na^+ \cdot N_2$ from a recent ab initio calculation,[44] then we obtain excellent agreement ($k = 1.2 \times 10^{-30}$ $(T/200\ K)^{-2.22}$) when the only adjusted parameters are $\langle\Delta E\rangle_{down}$, set to 200 cm^{-1}, and its temperature dependence expressed as T^n, where n is set to 0.45. Note that if the low-frequency bending modes of $Na^+ \cdot N_2$ are not treated as a free rotor, then the estimated rate coefficient is a factor 7.1−7.6 times slower over the temperature range 120−400 K and clearly in disagreement with experiment.

Using these parameters for $\langle\Delta E\rangle_{down}$ and n and molecular parameters for $Na^+ \cdot O_2$ from another ab initio calculation,[45] we obtain $k(Na^+ + O_2 + He) = 5.5 \times 10^{-31}$ $(T/200\ K)^{-2.26}$ cm^6 molecule^{-2} s^{-1}, which compares well with the measured result of $k = (5.20 \pm 2.62) \times 10^{-31}$ $(T/200\ K)^{-(2.64\ \pm\ 0.74)}$.[31] We therefore have some confidence in estimating k_4 and k_5 for the analogous reactions of K^+. The results are listed in Table 4. Note that the estimated value of k_5 is in accord with an upper limit of 2×10^{-30} cm^3 molecule^{-1} s^{-1} measured in a drift tube experiment.[24] For the association of K^+ and O, k_6 was estimated using the same parameters for $\langle\Delta E\rangle_{down}$ and n.

For the reactions $Na^+ + CO_2$ and $Na^+ + H_2O$, RRKM calculations using quantum calculations[46] on $Na^+ \cdot CO_2$ and $Na^+ \cdot H_2O$ agree satisfactorily with the measured rate coefficients[24,31] if $\langle\Delta E\rangle_{down}$ for He is set to 100 cm^{-1}, with n remaining as 0.45. The rate coefficient for reaction 8 is then 3.04×10^{-30} cm^6 molecule^{-2} s^{-1}, which is in good accord with the drift tube measurement of $(2.6 \pm 0.7) \times 10^{-30}$ cm^6 molecule^{-2} s^{-1}.[24] Although this value for $\langle\Delta E\rangle_{down}$ is still within the expected range for He as a third body,[43] it is half the value that produces the best RRKM fit to the reactions of Na^+ with N_2 and O_2 (see above). This does most likely not imply anything fundamentally different about the energy transfer processes involved in these reactions—rather, it indicates that the assumption of free rotors in the $Na^+ \cdot CO_2$ and $Na^+ \cdot H_2O$ complexes is an oversimplification. If the rotors are in fact partially hindered (resulting in slower rate coefficients), then our RRKM fit will be optimized with a larger $\langle\Delta E\rangle_{down}$, since this is the only adjustable parameter in the model.

The unimolecular dissociation rate coefficients, $k_{diss,0}$ were then estimated by detailed balance with $k_{rec,0}$, using the data in Table 1 to calculate the relevant equilibrium constants. The results are also listed in Table 5. Figure 2 illustrates $k_{rec,0}$ and $k_{diss,0}$ as a function of temperature for the five reactions. As expected, $k_{rec,0}$ is predicted to have a negative temperature dependence and is a function of the $K^+ \cdot X$ binding energy so that association with O_2 is slow and association with H_2O is fast. The slowest reaction is actually $K^+ + O$, because the $K^+ \cdot O$ adduct has only one vibrational mode and hence a relatively low density of rovibrational states. The dissociation rate coefficients have much larger (and positive) temperature dependences. Note that $k_{diss,0}$ for $K^+ \cdot N_2$ and $K^+ \cdot O_2$ is larger than 10^{-13} cm^3 molecule^{-1} s^{-1} at 200 K, so that these cluster ions will survive for less than 1 s at 95 km in the mesosphere.

TABLE 6: Rate Coefficients (in cm^3 molecule^{-1} s^{-1}) for K^+·X + Y → K^+·Y + X at 200 K[a]

X, Y	k_L^f	k^f	k_L^b	k^b	ΔH_0
O_2, O	2.9×10^{-10}	2.8×10^{-10}	6.5×10^{-10}	1.2×10^{-11}	−6.3
O, N_2	7.2×10^{-10}	2.5×10^{-11}	2.9×10^{-10}	2.9×10^{-10}	−0.7
O, CO_2	8.0×10^{-10}	7.1×10^{-10}	2.8×10^{-10}	2.3×10^{-14}	−17.7
O, H_2O	2.5×10^{-9}	7.1×10^{-10}	3.0×10^{-10}	5.2×10^{-21}	−47.8
O_2, N_2	6.9×10^{-10}	1.6×10^{-10}	6.3×10^{-10}	1.1×10^{-10}	−7.0
O_2, CO_2	7.6×10^{-10}	1.5×10^{-10}	6.1×10^{-10}	1.9×10^{-14}	−24.0
O_2, H_2O	2.5×10^{-9}	1.8×10^{-9}	6.5×10^{-10}	3.5×10^{-22}	−54.1
N_2, CO_2	7.8×10^{-10}	4.8×10^{-10}	6.8×10^{-10}	7.5×10^{-13}	−17.0
N_2, H_2O	2.5×10^{-9}	2.4×10^{-9}	7.1×10^{-10}	2.0×10^{-21}	−47.1
CO_2, H_2O	2.5×10^{-9}	1.4×10^{-9}	8.0×10^{-10}	5.7×10^{-16}	−30.1

[a] k_L^f and k_L^b are the Langevin rate coefficients for K^+·X + Y and K^+·Y + X, respectively. For reactions involving atomic O, an electronic degeneracy factor of 0.5 (at 200 K) is applied. k^f and k^b are the rate coefficients calculated from RRKM theory.

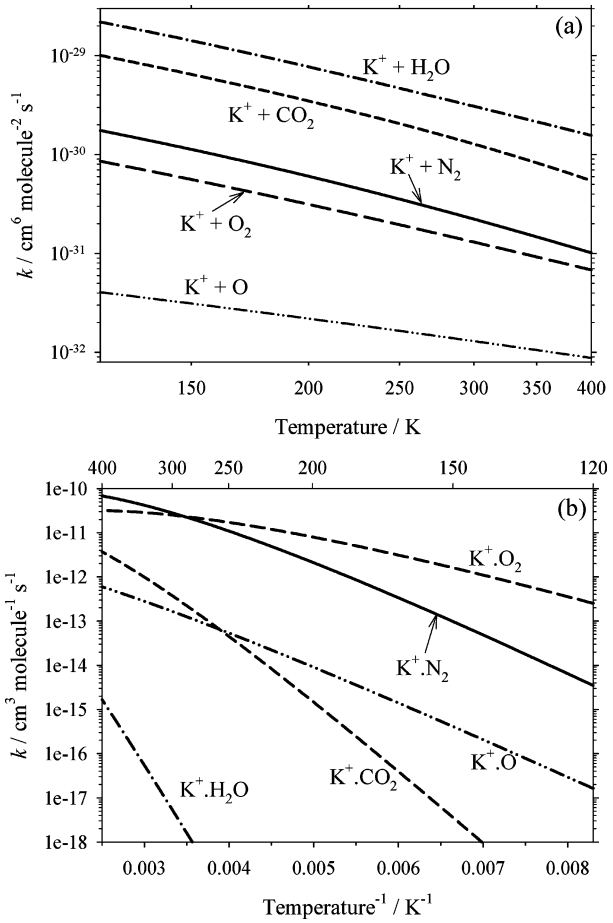

Figure 2. RRKM calculations with He as third body, using the data in Table 1: (a) plots of the low-pressure limiting rate coefficients versus temperature for the association of K^+ with N_2, O_2, O, CO_2, and H_2O; (b) plots of the low-pressure limiting dissociation rate coefficients for the corresponding cluster ions.

4. RRKM Calculations on the K^+·X + Y Ligand-Switching Reactions

The upper limit to the rate coefficient for a ligand-switching reaction of the form K^+·X + Y → K^+·Y + X is given by the Langevin limit, k^L (in cm^3 molecule^{-1} s^{-1}):

$$k_L = 9.5 \times 10^{-8} \sqrt{\frac{\alpha}{\mu}} \qquad \text{(I)}$$

Here α is the static polarizability in m^3 and μ is the reduced mass of the reactants in kg molecule^{-1}. If the reactant Y has a permanent dipole (e.g. H_2O), then k_L is increased by a factor that may be conveniently estimated using Troe's statistical adiabatic channel treatment.[42] However, the actual rate coefficient will be less than k_L if the reaction is endothermic or if the density of rovibrational states on the product side is less than on the reactant side.

We have previously[32] introduced a simple heuristic formalism to estimate switching rate coefficients, taking account of these effects. However, comparing the predictions of this formalism with a full RRKM calculation shows that it does not perform well in cases where a reaction involves a large change in the density of rovibrational states, particularly at low temperatures where the states need to be counted individually. In this study we have therefore applied RRKM theory to calculate a set of switching rate coefficients for 10 combinations of ligands X and Y appropriate to the upper atmosphere. These reactions are listed in Table 6 in the exothermic direction. The calculations were performed with the version of RRKM theory described above, where the microcanonical rate coefficients for dissociation of the Y·K^+·X intermediate to the reactants and products are determined using inverse Laplace transform to link them directly to their respective ion-capture rate coefficients, calculated using Langevin theory. Low-frequency degenerate bending vibrations (<80 cm^{-1}) in the cluster ions were treated as 2-dimensional free rotors when calculating the densities of rovibrational states. For reactions where Y = O, an electronic degeneracy factor was applied to reduce the Langevin rate constant. This is because the O·K^+·X complexes all have a degeneracy of 3, whereas O(^3P_J) has a minimum degeneracy of 5 O($^3P_2$), increasing with temperature as the higher spin−orbit multiplets become populated.

We now consider in detail two reactions that are central to the ion−molecule chemistry of K^+ in the MLT. The first reaction

$$K^+ \cdot N_2 + O \rightarrow KO^+ + N_2 \qquad (9)$$

is essentially thermoneutral ($\Delta H_0 = 0.7$ kJ mol^{-1}). In the case of the second reaction,

$$K^+ \cdot N_2 + CO_2 \rightarrow K^+ \cdot CO_2 + N_2 \qquad (10)$$

the CO_2·K^+·N_2 intermediate has a particularly high density of rovibrational states, with two internal 2-dimensional rotors. There is thus the possibility that association, at least in the endothermic direction (K^+·CO_2 + N_2), could be competitive with ligand-switching even at low pressures. Figure 3 illustrates the calculated rate coefficients (using $\langle \Delta E \rangle_{down} = 200$ cm^{-1}), both for the ligand-switching and association channels as a function of pressure. For reaction 9, association does not compete with switching until pressures above 10^4 Torr (Figure 3a). In contrast, for reaction 10 association in the endothermic direction (K^+·CO_2 + N_2) is faster than switching at pressures

TABLE 7: Neutral and Ionic Gas-Phase Reactions in the Potassium Model

no.	reacn	rate coeff[a]	source[b]
R1	$K + h\nu \rightarrow K^+ + e^-$	4×10^{-5}	1
R2	$K + NO^+ \rightarrow K^+ + NO$	9.4×10^{-10}	2
R3	$K + O_2^+ \rightarrow K^+ + O_2$	3.2×10^{-9}	2
R4	$K^+ + N_2 (+M) \rightarrow K^+ \cdot N_2$	$2.3 \times 10^{-30} (T/200)^{-2.39}$	3
R-4	$K^+ \cdot N_2 (+M) \rightarrow K^+ + N_2$	$2.8 \times 10^{-8} \exp(-1680/T)$	3
R5	$K^+ + O_2 (+M) \rightarrow K^+ \cdot O_2$	$1.2 \times 10^{-30} (T/200)^{-2.12}$	3
R-5	$K^+ \cdot O_2^+ (+M) \rightarrow K^+ + O_2$	$1.5 \times 10^{-9} \exp(-820/T)$	3
R6	$K^+ + O (+M) \rightarrow K^+ \cdot O^+$	$8.8 \times 10^{-32} (T/200\ \mathrm{K})^{-1.28}$	3
R-6	$K^+ \cdot O^+ (+M) \rightarrow K^+ + O$	$2.6 \times 10^{-10} \exp(-1800/T)$	3
R7	$K^+ + CO_2 (+M) \rightarrow K^+ \cdot CO_2$	$1.3 \times 10^{-29} (T/200)^{-2.43}$	3
R8	$K^+ + H_2O (+M) \rightarrow K^+ \cdot H_2O$	$3.0 \times 10^{-29} (T/200)^{-2.22}$	3
R9	$K^+ \cdot N_2 + O \rightarrow K^+ \cdot O + N_2$	$2.9 \times 10^{-10} (T/200\ \mathrm{K})^{-0.17}$	3
R-9	$K^+ \cdot O + N_2 \rightarrow K^+ \cdot N_2 + O$	$2.5 \times 10^{-11} (T/200\ \mathrm{K})^{-0.55}$	3
R10	$K^+ \cdot N_2 + CO_2 \rightarrow K^+ \cdot CO_2 + N_2$	$4.8 \times 10^{-10} (T/200\ \mathrm{K})^{-0.88}$	3
R-10	$K^+ \cdot CO_2 + N_2 \rightarrow K^+ \cdot N_2 + CO_2$	$2.8 \times 10^{-10} \exp(-2220/T)$	3
R11a	$K^+ \cdot O_2 + O \rightarrow K^+ \cdot O + O_2$	$2.8 \times 10^{-10} (T/200\ \mathrm{K})^{-0.42}$	3
R-11	$K^+ \cdot O + O_2 \rightarrow K^+ \cdot O_2 + O$	$5.0 \times 10^{-10} \exp(-752/T)$	3
R12	$K^+ \cdot O + CO_2 \rightarrow K^+ \cdot CO_2 + O$	$7.1 \times 10^{-10} (T/200\ \mathrm{K})^{-0.21}$	3
R-12	$K^+ \cdot CO_2 + O \rightarrow K^+ \cdot O + CO_2$	$1.4 \times 10^{-9} \exp(-2200/T)$	3
R13	$K^+ \cdot O + H_2O \rightarrow K^+ \cdot H_2O + O$	$7.1 \times 10^{-10} (T/200\ \mathrm{K})^{-1.90}$	3
R14	$K^+ \cdot O_2 + N_2 \rightarrow K^+ \cdot N_2 + O_2$	$1.6 \times 10^{-10} (T/200\ \mathrm{K})^{-0.90}$	3
R-14	$K^+ \cdot N_2 + O_2 \rightarrow K^+ \cdot O_2 + N_2$	$1.0 \times 10^{-9} \exp(-873/T)$	3
R15	$K^+ \cdot O_2 + CO_2 \rightarrow K^+ \cdot CO_2 + O_2$	$1.5 \times 10^{-10} (T/200\ \mathrm{K})^{-1.94}$	3
R16	$K^+ \cdot O_2 + H_2O \rightarrow K^+ \cdot H_2O + O_2$	$1.8 \times 10^{-9} (T/200\ \mathrm{K})^{-0.99}$	3
R17	$K^+ \cdot N_2 + H_2O \rightarrow K^+ \cdot H_2O + N_2$	$2.4 \times 10^{-9} (T/200\ \mathrm{K})^{-0.45}$	3
R18	$K^+ \cdot CO_2 + H_2O \rightarrow K^+ \cdot H_2O + CO_2$	$1.4 \times 10^{-9} (T/200\ \mathrm{K})^{-1.26}$	3
R19	$K^+ \cdot X + e^- \rightarrow K + X$ (X = N_2, O_2, CO_2, H_2O and O)	$1 \times 10^{-6} (T/200)^{-1/2}$	4

[a] Rate coefficient units: unimolecular, s^{-1}; bimolecular, cm^3 molecule^{-1} s^{-1}; termolecular, cm^6 molecule^{-2} s^{-1}. [b] Key: (1) Swider;[34] (2) scaled from the analogous Na reactions (see text); (3) calculated from RRKM theory; (4) estimated.[2]

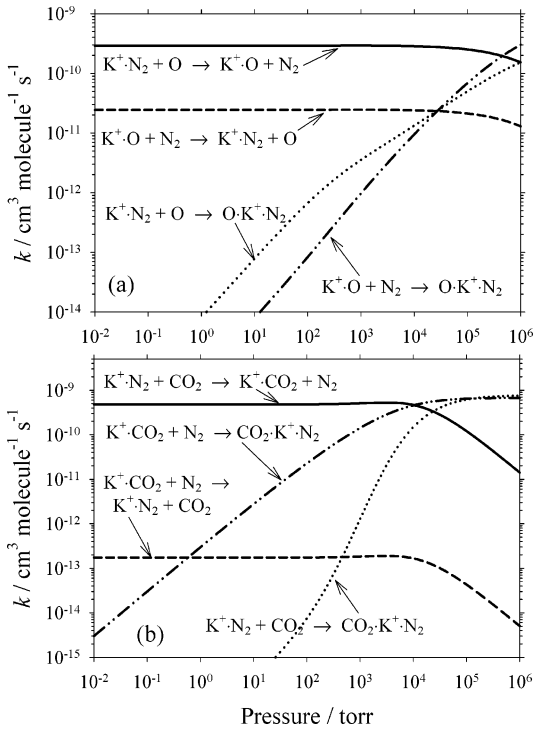

Figure 3. RRKM calculations of the rate coefficients at 200 K for (a) the $K^+ \cdot N_2 + O \leftrightarrow K^+ \cdot O + N_2$ system and (b) the $K^+ \cdot N_2 + CO_2 \leftrightarrow K^+ \cdot CO_2 + N_2$ system, showing the ligand-switching and association channels as a function of pressure.

above 0.5 Torr (Figure 3b). However, this is more than 3 orders of magnitude higher than the pressure in the MLT, where association should therefore be negligible.

Table 6 compares the ligand-switching rate coefficients predicted by RRKM theory at 200 K and a pressure of 10^{-3} Torr, with the Langevin capture rate constants. For half of the ligand combinations, the rate coefficients in the exothermic direction are within 50% of their Langevin capture rate constants, and all but one are within 20%. For the final reaction, $K^+ \cdot O + N_2 \rightarrow K^+ \cdot N_2 + O$, the rate coefficient is only 3% of the Langevin rate constant (see Figure 3a). The reason is that the density of rovibrational states of the products is nearly 1 order of magnitude lower than that of the reactants. This arises for two reasons. First is the reduction in rotational degrees of freedom, from 2 to 1. Second, in $K^+ \cdot N_2$ the degenerate bending frequencies are relatively high (177 cm^{-1}); since the reaction is essentially thermoneutral (-0.7 kJ mol^{-1}), there will be little energy available for internal excitation of $K^+ \cdot N_2$, so we have not treated the N_2 as a free rotor. Note that if the degenerate bending modes are treated as free rotors, $k(K^+ \cdot O + N_2)$ increases to $2.8 \times 10^{-10} (T/200\ \mathrm{K})^{-0.32}$, which is 40% of the Langevin capture rate, but this has very little effect on the atmospheric model results described below.

5. Atmospheric Modeling

The full set of reactions required to model the ion−molecule chemistry of potassium in the MLT are listed in Table 7. The charge-transfer reactions that produce K^+ (reactions 2 and 3) do not appear to have been studied. Their rate coefficients were therefore estimated by taking the measured rate coefficients for the analogous reactions of Na with NO^+ and O_2^+ [47] and scaling by a factor of 1.2 to take account of the relative Langevin collision frequencies of K and Na with these ions. Reactions 4−8 are the association reactions that form the primary cluster ions, of which reaction 4 is dominant because of the high concentration of atmospheric N_2. The RRKM calculations in section 3 were made with He as the third body, for comparison with laboratory measurements. To take account of the higher relative efficiency of N_2 (and O_2) as a third body in the atmosphere, the rate coefficients of reactions 4, −4, 5, −5, 6, −6, 7, and 8 are multiplied by a factor of 4. This factor is based on an extensive literature survey of the relative efficiencies of N_2 and He.[30]

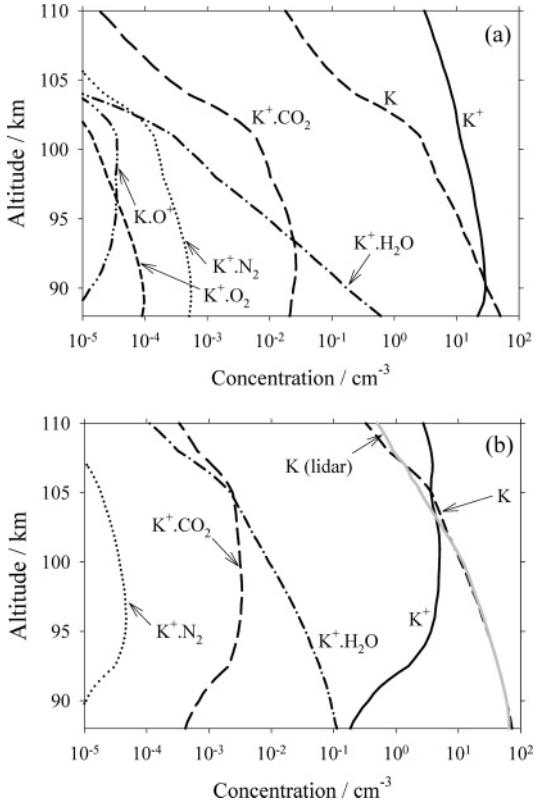

Figure 4. Predicted vertical profiles of K, K^+, and the K^+ cluster ions at 40° N in January: (a) midday; (b) midnight. The gray line indicates nighttime lidar measurements of K from ref 2.

Reactions 9−18 are a subset of the ligand-switching reactions considered in section 4. The omitted reactions are too slow to be significant in the MLT because of their large activation energies. Note that in addition to ligand-switching, the reactions K^+·O + O_2 and K^+·O_2 + O could undergo exothermic chemical reactions to form $K^+ + O_3$. Similarly, the reaction K^+·O + O could produce $O_2(a^1\Delta_g$ and $b^1\Sigma_g^+$, if spin is conserved). However, the concentrations of K^+·O and K^+·O_2 are predicted to be so low in the atmosphere, because of their thermal instability, that the model is not sensitive to these reactions even if they occur at the collision rate. Reaction 20 encompasses the group of electron recombination reactions K^+·X + e^- → K + X. None of these dissociative recombination reactions appears to have been studied, so k_{20} is set to a value and temperature dependence typical for this type of reaction.[48]

The distribution of K-containing ions in the MLT is now modeled by inserting this set of reactions into our 1-dimensional model of potassium,[2] updated with the diurnally resolved temperature profile measured by a Na lidar.[49] As an example, we show results for midlatitudes (40−55° N) in January. Figure 4 illustrates the predicted profiles of K, K^+, and the molecular K^+ ions at midday and midnight. K^+, K^+·CO_2, and K^+·H_2O are predicted to be the dominant ions. The large diurnal variation of K above 100 km is due to the daytime conversion of K to K^+, which is caused by the 1 order of magnitude increase in NO^+ and O_2^+ (reactions 2 and 3), and photoionization. Below 100 km, K^+ exhibits a large diurnal variation, becoming severely depleted at night. However, it is important to note that this model provides a steady-state solution of the potassium chemistry; that is, the chemistry readjusts instantaneously as the densities of species such as atomic O, major ions, and electrons and temperature vary over a diurnal cycle. The midday and midnight profiles in Figure 4 are therefore limiting cases: as we will show below, the time constants in the potassium chemistry become quite long (>1 day) above 100 km, so that the diurnal variations will be smaller than in Figure 4.

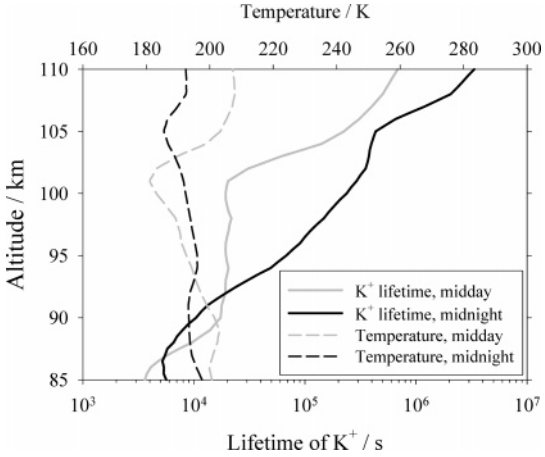

Figure 5. Predicted profiles of the lifetime of K^+ against neutralization to K (full lines) and the atmospheric temperature (broken lines): midday (gray); midnight (black).

Measurements of ions in the MLT have been made by rocket-borne mass spectrometry since the 1960s, and K^+ has been assigned to mass 39.[16−20] Although this mass could also be NaO^+, we have shown previously[32] that this ion should have a concentration well below 0.1 cm^{-3}. The small number of K^+ measurements that have been published show a broad peak in the ion profile between about 95 and 100 km, with peak concentrations of 20−100 cm^{-3}, and some evidence of K^+ below 90 km in daytime.[18,19] These concentrations are in sensible accord with the model predictions in Figure 4. Figure 4b includes a plot of the nighttime average atomic K profile measured by lidar at 54° N in January.[2] This profile compares very well with the model prediction.

Figure 5 illustrates the predicted lifetime of K^+ against neutralization to K, as a function of height for midday and midnight. This plot demonstrates that the K^+ lifetime varies by more than 2 orders of magnitude, from about 2 h at 85 km to nearly 1 month at 110 km. Comparison with our study on Na^+[32] shows that the lifetime of K^+ is about 200 times longer around 90 km. This is because of the rapid thermal dissociation of molecular ions such as K^+·N_2, which competes with ligand-switching or dissociative recombination with electrons. In contrast, the Na^+ molecular ions are more stable (by about 12 kJ mol^{-1} in the case of Na^+·N_2).

The K^+ lifetime is therefore a complex function of [e^-], [O], and temperature (because of the strong *T*-dependences of k_{-4}, k_{-5}, and k_{-6}). Above 95 km, the midday lifetime is roughly 10−20 times shorter than at midnight, because [e^-] is about 1 order of magnitude larger. However, below 90 km, the daytime lifetime is actually longer because of the large increase in [O] during the day between 80 and 90 km: reaction 9 (K^+·N_2 + O) then competes with reaction 10 (K^+·N_2 + CO_2), thereby preventing the formation of the more stable clusters. Note that the midday lifetime profile exhibits a pronounced minimum just above 100 km, which corresponds to a minimum in the temperature profile (Figure 5). This behavior is explained by the decrease in the thermal dissociation rates of the weakly bound K^+ clusters at the lower temperatures.

6. Conclusions

High-level ab initio calculations have provided the input for RRKM calculations to estimate the rate coefficients for a series of association and ligand-switching reactions that should govern

the ion−molecule chemistry of K^+ in the MLT. The results show that K^+ does not form strongly bound clusters (or chemical bonds) with N_2, O_2, or O, unlike the other metallic ions that occur in the MLT and have been studied in the laboratory (e.g. Fe^+, Mg^+, Na^+, Ca^+). This property prevents K^+ forming clusters which are sufficiently long-lived to switch with CO_2 or H_2O and then undergo dissociative recombination with electrons. The result is that K^+ should have a much longer lifetime than these other metallic ions in the upper atmosphere. Note that the failure of the simple formalism[32] for predicting ligand-switching rate constants will have some implications for our previous study of sodium ion chemistry in the mesosphere; however, the effects are not expected to be very large because the important switching reactions between N_2 and O were treated by full RRKM theory.

Finally, we consider the impact of this chemistry on a K_s layer forming from the K^+ ions in a descending sporadic E layer. With extrapolation from our work on Na_s and Fe_s layers, a K_s layer will be triggered by a sharp decrease of K^+ lifetime with decreasing altitude. Interestingly, K^+ lifetimes should be much more variable compared to Na^+ and Fe^+ lifetimes. This is because the Na^+ lifetime above 90 km is largely governed only by [O],[30,32] and the Fe^+ lifetime by both [O] and [e^-],[50] but the K^+ lifetime is governed by both these parameters *and* the local temperature. Thus a K_s layer might not appear together with a Na_s and Fe_s layer unless a sporadic E layer descended into a cold region, for instance produced by an atmospheric gravity wave.[1] An experiment where lidar observations were made of the K and either Na or Fe density, temperature (from high-resolution lidar measurements of one of the metals[1]), and electron density measurements with an incoherent scatter radar[28] would provide a detailed test of the predictions of this ion−molecule scheme. Finally, laboratory studies are required of the association reactions of K^+, as well as of the reactions of the resulting K^+ cluster ions—thermal dissociation, ligand-switching, and recombination with electrons.

Acknowledgment. The authors are grateful to the EPSRC for the award of computer time at the Rutherford Appleton Laboratories under the auspices of the Computational Chemistry Working Party (CCWP), which enabled these calculations to be performed. Dr. E. P. F. Lee (Southampton) is thanked for his input to the earlier calculations.

References and Notes

(1) Plane, J. M. C. *Chem. Rev.* **2003**, *103*, 4963.
(2) Eska, V.; von Zahn, U.; Plane, J. M. C. *J. Geophys. Res., Space Phys.* **1999**, *104*, 17173.
(3) Hunten, D. M. *Space Sci. Rev.* **1967**, *6*, 493.
(4) Gault, W. A.; Chanin, M. L. *Ann. Geophys.* **1974**, *30*, 369.
(5) Sullivan, H. M.; Hunten, D. M. *Can. J. Phys.* **1964**, *42*, 937.
(6) Eska, V.; Hoffner, J.; von Zahn, U. *J. Geophys. Res., Space Phys.* **1998**, *103*, 29207.
(7) Fricke-Begemann, C.; Hoffner, J.; von Zahn, U. *Geophys. Res. Lett.* **2002**, *29*, art. no. 2067.
(8) Megie, G.; Bos, F.; Blamont, J. E.; Chanin, M. L. *Planet. Space Sci.* **1978**, *26*, 27.
(9) Raizada, S.; Tepley, C. A.; Janches, D.; Friedman, J. S.; Zhou, Q.; Mathews, J. D. *J. Atmos. Sol.-Terr. Phys.* **2004**, *66*, 595.
(10) Tepley, C. A.; Raizada, S.; Zhou, Q. H.; Friedman, J. S. *Geophys. Res. Lett.* **2003**, *30*, art. no. 1009.
(11) Friedman, J. S.; Tepley, C. A.; Raizada, S.; Zhou, Q. H.; Hedin, J.; Delgado, R. *J. Atmos. Sol.-Terr. Phys.* **2003**, *65*, 1411.
(12) von Zahn, U.; Hoffner, J.; McNeil, W. J. Meteor trails as observed by lidar. In *Meteors in the earth's atmosphere*; Murad, E., Williams, I. P., Eds.; Cambridge University Press: Cambridge, U.K., 2002; p 149.
(13) von Zahn, U.; Gerding, M.; Hoffner, J.; McNeil, W. J.; Murad, E. *Meteor. Planet. Sci.* **1999**, *34*, 1017.
(14) Hoffner, J.; von Zahn, U.; McNeil, W. J.; Murad, E. *J. Geophys. Res., Space Phys.* **1999**, *104*, 2633.
(15) Gerding, M.; Alpers, M.; Hoffner, J.; von Zahn, U. *J. Geophys. Res., Space Phys.* **1999**, *104*, 24689.
(16) Kopp, E.; Eberhardt, P.; Herrmann, U.; Bjorn, L. G. *J. Geophys. Res., Atmos.* **1985**, *90*, 3041.
(17) Kopp, E. *J. Geophys. Res.* **1997**, *102*, 9667.
(18) Zbinden, P. A.; Hidalgo, M. A.; Eberhardt, P.; Geiss, J. *Planet. Space Sci.* **1975**, *23*, 1621.
(19) Aikin, A. C.; Goldberg, R. A. *J. Geophys. Res.* **1973**, *78*, 734.
(20) Balsiger, F.; Kopp, E.; Friedrich, M.; Torkar, K. M.; Walchli, U.; Witt, G. *Geophys. Res. Lett.* **1996**, *23*, 93.
(21) Goldberg, R. A.; Aikin, A. C. *Science* **1973**, *180*, 294.
(22) Grebowsky, J. M.; Aikin, A. C. In situ measurements of meteoric ions. In *Meteors in the earth's atmosphere*; Murad, E., Williams, I. P., Eds.; Cambridge University Press: Cambridge, U.K., 2002; p 189.
(23) Ferguson, E. E.; Fehsenfeld, F. C. *J. Geophys. Res.* **1968**, *73*, 6215.
(24) Johnsen, R.; Brown, H. L.; Biondi, M. A. *J. Chem. Phys.* **1971**, *55*, 186.
(25) Clemesha, B. R. *J. Atmos. Terr. Phys.* **1995**, *57*, 725.
(26) Von Zahn, U.; Hansen, G.; Kurzawa, H. *Nature* **1988**, *331*, 594.
(27) Kane, T. J.; Gardner, C. S.; Zhou, Q.; Mathews, J. D.; Tepley, C. A. *J. Atmos. Terr. Phys.* **1993**, *55*, 499.
(28) Collins, S. C.; Plane, J. M. C.; Kelley, M. C.; Wright, T. G.; Soldan, P.; Kane, T. J.; Gerrard, A. J.; Grime, B. W.; Rollason, R. J.; Friedman, J. S.; Gonzalez, S. A.; Zhou, Q. H.; Sulzer, M. P.; Tepley, C. A. *J. Atmos. Sol.-Terr. Phys.* **2002**, *64*, 845.
(29) Heinselman, C. J.; Thayer, J. P.; Watkins, B. J. *Geophys. Res. Lett.* **1998**, *25*, 3059.
(30) Cox, R. M.; Plane, J. M. C. *J. Geophys. Res., Atmos.* **1998**, *103*, 6349.
(31) Cox, R. M.; Plane, J. M. C. *J. Chem. Soc., Faraday Trans.* **1997**, *93*, 2619.
(32) Daire, S. E.; Plane, J. M. C.; Gamblin, S. D.; Soldan, P.; Lee, E. P. F.; Wright, T. G. *J. Atmos. Sol.-Terr. Phys.* **2002**, *64*, 861. (Note that an erroneous version of this paper was published in the same journal (**2002**, *64*, 443): it was reprinted by the publishers, owing to uncorrected errors by them at the proof stage.)
(33) Dressler, R. A.; Murad, E. The Gas-phase chemical dynamics associated with meteors. In *Chemical Dynamics in Extreme Environments*; Dressler, R. A., Ed.; World Science: Singapore, 2001; p 268.
(34) Swider, W. *Annal. Geophys.* **1970**, *26*, 595.
(35) Hunten, D. M. *Geophys. Res. Lett.* **1981**, *8*, 369.
(36) Bates, D. R.; Dalgarno, A. *Atomic and Molecular Processes*; Academic Press: New York, 1962.
(37) Lee, E. P. F.; Almahdi, Z.; Musgrave, A.; Wright, T. G. *Chem. Phys. Lett.* **2003**, *373*, 599.
(38) Lee, E. P. F.; Wright, T. G. *Chem. Phys. Lett.* **2002**, *363*, 139.
(39) Lee, E. P. F.; Wright, T. G. *J. Phys. Chem. A* **2003**, *107*, 7024.
(40) De Avillez Pereira, R.; Baulch, D. L.; Pilling, M. J.; Robertson, S. H.; Zeng, G. *J. Phys. Chem. A* **1997**, *101*, 9681.
(41) Plane, J. M. C.; Rollason, R. J. *J. Phys. Chem. A* **2001**, *105*, 7047.
(42) Troe, J. *J. Chem. Phys.* **1987**, *87*, 2773.
(43) Gilbert, R. G.; Smith, S. C. *Theory of Unimolecular and Recombination Reactions*; Blackwell: Oxford, U.K., 1990.
(44) Soldan, P.; Spirko, V.; Lee, E. P. F.; Wright, T. G. *J. Chem. Phys.* **1999**, *111*, 3420.
(45) Lee, E. P. F.; Soldan, P.; Wright, T. G. *Chem. Phys. Lett.* **1999**, *301*, 317.
(46) Soldan, P.; Lee, E. P. F.; Gamblin, S. D.; Wright, T. G. *Chem. Phys. Lett.* **1999**, *313*, 379.
(47) Levandier, D. J.; Dressler, R. A.; Williams, S.; Murad, E. *J. Chem. Soc., Faraday Trans.* **1997**, *93*, 2611.
(48) Rees, M. H. *Physics and Chemistry of the Upper Atmosphere*; Cambridge University Press: Cambridge, U.K., 1989.
(49) States, R. J.; Gardner, C. S. *J. Atmos. Sci.* **2000**, *57*, 78.
(50) Plane, J. M. C.; Self, D. E.; Vondrak, T.; Woodcock, K. R. I. *Adv. Space Res.* **2003**, *32*, 699.